AIAA JOURNAL
Vol. 38, No. 1, January 2000

Structural Modeling of Parachute Dynamics

Michael Accorsi* and John Leonard†
University of Connecticut, Storrs, Connecticut 06269-2037
and
Richard Benney‡ and Keith Stein‡
U.S. Army Soldier and Biological Chemical Command, Natick, Massachusetts 01760-5017

The dynamic behavior of parachute systems is an extremely complex phenomenon characterized by nonlinear, time-dependent coupling between the parachute and surrounding airflow, large shape changes in the parachute, and three-dimensional unconstrained motion of the parachute through the fluid medium. Because of these complexities, the design of parachutes has traditionally been performed using a semi-empirical approach. This approach to design is time consuming and expensive. The ability to perform computer simulations of parachute dynamics would significantly improve the design process and ultimately reduce the cost of parachute system development. The finite element formulation for a structural model capable of simulating parachute dynamics is presented. Explicit expressions are given for structural mass and stiffness matrices and internal and external force vectors. Algorithms for solution of the nonlinear dynamic response are also given. The capabilities of the structural model are demonstrated by three example problems. In these examples, the effect of the surrounding airflow is approximated by prescribing the canopy pressure and by applying cable and payload drag forces on the structural model. The examples demonstrate the ability to simulate three-dimensional unconstrained dynamics beginning with an unstressed folded configuration corresponding to the parachute cut pattern. The examples include simulations of the inflation, terminal descent, and control phases.

Nomenclature

${}^{\prime}A$, A	= determinant of metric tensors ${}^{\prime}A_{\alpha\beta}$ and $A_{\alpha\beta}$, respectively
${}^{\prime}A_{\alpha\beta}$, $A_{\alpha\beta}$	= covariant metric tensors of ${}^{\prime}C$ and ${}^{\circ}C$, respectively
${}^{\prime}A^{\alpha\beta}$, $A^{\alpha\beta}$	= contravariant metric tensors of ${}^{\prime}C$ and ${}^{\circ}C$, respectively
$C^{\alpha\beta\lambda\mu}$	= material constitutive tensor
${}^{\prime}D_{Ni}$	= Cartesian displacements of node N on element from ${}^{\circ}C$ to ${}^{\prime}C$
$\dot{D}_{Ni}$	= Cartesian velocities of node N on element in ${}^{\prime}C$
$\ddot{D}_{Ni}$	= Cartesian accelerations of node N on element in ${}^{\prime}C$
$\{{}^{\#}D\}$, $\{{}^{\#}\tilde{D}\}$	= correct and estimated displacement vector of nodes from ${}^{\circ}C$ to ${}^{\prime}C$, respectively
E	= Young's modulus
$\hat{\boldsymbol{e}}_i$	= unit base vectors in Cartesian directions
e_{ijk}	= permutation symbol
${}^{\prime}F_{Ni}$	= discretized external force on node N
$H_N(x_\alpha)$	= polynomial shape function of x_α
h	= thickness of membrane
$[K_{\text{eff}}]$	= effective stiffness matrix for Newmark method
$[{}^{\#}\tilde{K}]$	= estimated tangent stiffness matrix on ${}^{\#}C$
M_{MNij}	= mass matrix connecting nodes M and N
${}^{\prime}\hat{N}$	= unit normal to ${}^{\prime}C$
${}^{\prime}n^{\alpha\beta}$, ${}^{\#}n^{\alpha\beta}$	= Kirchhoff stress resultant tensors on ${}^{\prime}C$ and ${}^{\#}C$, respectively
p	= net pressure on canopy
${}^{\prime}p_i$	= Cartesian components of tractions on ${}^{\prime}C$
${}^{\prime}R_{Ni}$	= discretized internal restoring force on node N
t	= time
${}^{\prime}u_i$	= Cartesian displacements of point to ${}^{\prime}C$ from ${}^{\circ}C$
${}^{\prime}\dot{u}_i$	= Cartesian accelerations of point to ${}^{\prime}C$ from ${}^{\circ}C$
x_α	= nondimensional curvilinear coordinates in element
$\tilde{Y}_{Ni}$	= Cartesian coordinates of node N on element in ${}^{\circ}C$
y_i	= Cartesian coordinates of a point on ${}^{\circ}C$
${}^{\prime}y_i$	= Cartesian coordinates of a point on ${}^{\prime}C$
α, β	= Newmark parameters
${}^{\prime}\gamma_{\alpha\beta}$	= Green strain tensor
$\{{}^{\#}\Delta D\}$	= correction vector to estimate $\{{}^{\#}\tilde{D}\}$
Δt	= time step
δ_{ij}	= Kronecker delta
δu_i	= virtual displacements
η, λ	= damping parameters
ν	= Poisson's ratio
ξ, ω	= damping ratio and natural frequency of a particular mode of free vibration
ρ	= mass density of ${}^{\circ}C$

Received 1 October 1998; revision received 5 May 1999; accepted for publication 11 May 1999.

*Associate Professor, Department of Civil and Environmental Engineering; accorsi@engr.uconn.edu.
†Professor, Department of Civil and Environmental Engineering.
‡Aerospace Engineer, Soldier Systems Center.

I. Introduction

PARACHUTE deployment, inflation, and terminal descent are extremely difficult aerodynamic phenomena to model. These processes are governed by coupled, nonlinear, time-dependent equations for the interaction of the fluid medium and parachute. Because of these complexities, it is not surprising that the design of parachutes has historically been performed using semi-empirical methods.[1]

During the past two decades, the demands placed on parachute designers have increased tremendously. Payload costs have increased, mission requirements have become more stringent, and the flight tests needed to design new parachute systems have become more costly. In light of these demands, the traditional semi-empirical approach to parachute design is inadequate. Computational methods have the greatest potential for providing the necessary predictive models for parachute design.

The three phases that occur during a parachute mission are deployment, inflation, and terminal descent with precision soft landing.[2] The deployment phase is a highly nonlinear process in which the parachute and suspension lines unfold from the deployment bag. In the inflation phase, airflow causes large canopy shape changes as the parachute is stressed and begins to decelerate. This phase is also highly nonlinear, and maximum forces typically occur during this time. The terminal descent phase corresponds to all behavior following inflation and may include various control operations performed on the parachute system. In general, all three phases involve strong coupling between the parachute system and surrounding airflow.

Computer simulations of all three phases are needed to fully characterize the behavior of a given parachute system under given conditions. In general, comprehensive simulations require coupling of structural dynamics (SD) and computational fluid dynamic (CFD) models to capture the true aerodynamic behavior, however, valuable information can be obtained from either standalone SD or CFD simulations. The finite element method (FEM) is most commonly used for the SD model and grid-based CFD and vortex element methods are both used for fluid modeling. Standalone SD simulations are performed by prescribing the canopy pressure and aerodynamic drag on the parachute components and are computationally efficient because the SD model is usually considerably smaller than the required CFD model. For standalone CFD simulations, the parachute geometry is prescribed, and the surrounding airflow is calculated. The calculated surface loads are then used to derive global parachute motion.

II. Previous Work

Deployment has been successfully simulated by Purvis[3] using a discrete element model similar to Sundberg.[4] In that axisymmetric model, the partially deployed canopy and suspension lines are modeled as elastically connected, lumped mass nodes, and semiempirical parameters account for aerodynamic forces. Although improvements to this model are possible, three-dimensional finite element modeling of the initial deployment process have not yet been performed.

Significant progress has recently been made on simulation of the parachute inflation and terminal descent phases. Coupled inflation simulations of axisymmetric parachutes have been presented by Haug et al.[5] and Stein et al.[6] Three-dimensional standalone SD inflation simulations have been presented by Mosseev[7] and Benney et al.[8] Standalone CFD models have been used to predict the flowfield in the terminal descent phase surrounding a canopy with prescribed geometry. This type of analysis has been performed for round parachutes,[9] round parachute clusters,[10] and parafoils.[11,12] Standalone SD simulations of cross and round parachutes and parafoils in terminal descent have been demonstrated by Benney et al.[8] Coupled simulations of the terminal descent phase beginning with an inflated canopy shape have recently been performed by Nelsen,[13] Stein et al.,[14] and Benney et al.[15]

In summary, the ability to perform standalone SD inflation simulations has been demonstrated by several researchers. Standalone CFD predictions of the flowfield surrounding a parachute with a prescribed rigid shape are generally available. Coupled dynamic and deformable inflation simulations have been very limited. Coupled simulations of the terminal descent phase beginning with an inflated canopy shape have recently been achieved by several researchers. To date, detailed simulation of the initial deployment phase has not been addressed. There still exists a tremendous need to perform coupled dynamic simulations of all three phases of a parachute dynamics problem.

The purpose of this paper is to present the theoretical foundations for an SD model capable of simulating parachute deployment, inflation, and terminal descent. This model is being developed jointly by researchers at the U.S. Army Soldier Systems Command, Natick Research, Development, and Engineering Center, and the University of Connecticut, and a parallel version of the model is being coupled with a CFD model developed by researchers at the Army High Performance Computing Research Center at Rice University. The structural theory has been incorporated into a finite element code that is highly tailored for parachute simulations. Several standalone SD simulations are presented to demonstrate the capabilities of this structural code. The example problems are rather complex, and corresponding experimental data are not readily available. The predictions of the coupled model have recently been compared with experiments and good agreement was obtained.[16]

III. SD Theory

In this section we consider the nonlinear dynamic behavior of thin, extremely flexible, and cable-reinforced membranes using the FEM.[17,18] Isoparametric elements[19] are used to develop discretized equations of motion admitting large dynamic displacements. A total Lagrangian[19] coordinate system is adopted, with curvilinear local coordinates embedded in the reference surface. The nonlinear dynamic responses are integrated in time using an implicit Newmark method.[19]

In the following, capital Latin letters as indices denote nodal variables on an element. Greek indices take on the values 1 and 2 on the surface, and lower case Latin indices take on the values 1, 2, and 3. A repeated index indicates summation over the range of the index. Commas used as subscripts denote partial differentiation with respect to the coordinate component with the succeeding index. A special notation is adopted to identify various configurations of the membrane: A leading superscript on a variable denotes the surface on which the variable is defined. The reference surface where magnitudes and orientations of the variables are defined is the initial unstrained state ${}^{\circ}C$. Thus, we will arrive at a total Lagrangian description of the nonlinear equations at time t on surface ${}^{t}C$, or at time $t + \Delta t$ on ${}^{\#}C$.

A. Geometric Interpolation

The simultaneous interpolation of geometry as well as displacements by the same shape functions, that is, isoparametric interpolation, can be used for curved cables and membranes. We specify curvilinear coordinates x_1 and x_2 on the reference surface ${}^{\circ}C$ to be nondimensional natural coordinates and assume the Cartesian coordinates y_i and displacements ${}^{t}u_i$ at a generic point in the element to be given by

$$y_i(x_\alpha) = H_N(x_\alpha) Y_{iN} \tag{1a}$$

$${}^{t}u_i(x_\alpha) = H_N(x_\alpha)\, {}^{t}D_{iN} \tag{1b}$$

where $H_N(x_\alpha)$ are the element shape functions. We adopt polynomial shape functions that map a general quadrilateral or triangular surface element curved in three-dimensional space onto two-dimensional squares or triangles.

As the surface of the membrane deforms from the unstrained state ${}^{\circ}C$ to ${}^{t}C$ at time t we write the time-varying coordinates as

$${}^{t}y_i = y_i + {}^{t}u_i \tag{2a}$$

Because the metric tensor of a differential arc length in ${}^{t}C$ relative to ${}^{\circ}C$ is given by[20] [using Eqs. (1)]

$${}^{t}A_{\alpha\beta} = {}^{t}y_{i,\alpha} \cdot {}^{t}y_{i,\beta} = H_{N,\alpha} H_{M,\beta} (Y_{iN} + {}^{t}D_{iN})(Y_{iM} + {}^{t}D_{iM}) \tag{2b}$$

and because the Green strain tensor[20] of a differential arc length on ${}^{t}C$ relative to ${}^{\circ}C$ is

$$\begin{aligned} {}^{t}\gamma_{\alpha\beta} &= \frac{{}^{t}A_{\alpha\beta} - A_{\alpha\beta}}{2} \\ &= H_{N,\alpha} H_{M,\beta} \frac{Y_{iN}\, {}^{t}D_{iM} + Y_{iM}\, {}^{t}D_{iN} + {}^{t}D_{iN}\, {}^{t}D_{iM}}{2} \end{aligned} \tag{3}$$

the stress resultant tensor for a Hookean material is

$${}^{t}n^{\alpha\beta} = C^{\alpha\beta\lambda\mu}\, {}^{t}\gamma_{\lambda\mu} \tag{4}$$

where for an isotropic material in plane stress[20]

$$C^{\alpha\beta\lambda\mu} = \frac{hE\nu}{(1-\nu^2)} A^{\alpha\beta} A^{\lambda\mu} + \frac{hE}{2(1+\nu)} (A^{\alpha\lambda} A^{\beta\mu} + A^{\alpha\mu} A^{\beta\lambda}) \tag{5}$$

B. Equations of Motion

We will develop the discretized equations of motion in terms of an arbitrary constitutive equation that will allow several existing material models to be used; Eq. (5) is a particular example. The equations of motion can be developed from the principle of virtual work as written on the dynamic equilibrium state ${}^{t}C$ but referred to ${}^{\circ}C$ as[17]

$$\begin{aligned} 0 = &\int\int ({}^{t}n^{\alpha\beta}\, \delta\gamma_{\alpha\beta} - {}^{t}p_i\, \delta u_i) \sqrt{A}\, \mathrm{d}x_1\, \mathrm{d}x_2 \\ &+ h \int\int \rho\, {}^{t}\ddot{u}_i\, \delta u_i \sqrt{A}\, \mathrm{d}x_1\, \mathrm{d}x_2 \end{aligned} \tag{6}$$

where $\delta\gamma_{\alpha\beta}$ is the infinitesimal virtual strain corresponding to a small virtual displacement δu_i superposed on ${}'C$, and the force vector

$$\bar{\boldsymbol{F}}\sqrt{{}'A}\,\mathrm{d}x_1\,\mathrm{d}x_2 = {}'p_i\sqrt{A}\,\mathrm{d}x_1\,\mathrm{d}x_2\hat{\boldsymbol{e}}_i \tag{7}$$

has been expressed in terms of Cartesian components ${}'p_i$.

In a consistent mass approach, the accelerations are given by

$${}'\ddot{u} = H_N\,{}'\ddot{D}_{Ni} \tag{8}$$

Then substitute Eqs. (1), (3), and (8) into Eq. (6) to obtain for an arbitrary virtual displacement δD_{Mi} the following discretized equation of motion for the ith force component at the Nth node:

$$M_{MNij}\,{}'\ddot{D}_{Mj} + {}'R_{Ni} = {}'F_{Ni} \tag{9a}$$

where the mass matrix is

$$M_{MNij} = \delta_{ij}\rho h\int\int H_N H_M\sqrt{A}\,\mathrm{d}x_1\,\mathrm{d}x_2 \tag{9b}$$

the internal restoring force is

$${}'R_{Ni} = \frac{1}{2}\int\int {}'n^{\alpha\beta}(H_{M,\alpha}H_{N,\beta} + H_{N,\alpha}H_{M,\beta})\sqrt{A}\,\mathrm{d}x_1\,\mathrm{d}x_2 \times(Y_{Mi} + {}'D_{Mi}) \tag{9c}$$

and the external force is

$${}'F_{Ni} = \int\int {}'p_i H_N\sqrt{A}\,\mathrm{d}x_1\,\mathrm{d}x_2 \tag{9d}$$

Note that $\sqrt{A}$ in Eqs. (9) can be obtained from Eq. (2b) in terms of derivatives of the shape functions and the nodal coordinates, thus, further complicating the integration required to form the element matrices.

Equations (9) represent a set of ordinary differential equations of dynamic equilibrium at time t of every degree of freedom on ${}'C$. Equations (9) are nonlinear in that 1) material nonlinearities are possible in the restoring force ${}'R_{Ni}$ because ${}'n^{\alpha\beta}$ can be replaced by any constitutive equation; 2) ${}'R_{Ni}$ is nonlinear even if the constitutive equation is linear because ${}'R_{Ni}$ includes finite displacement components ${}'D_{Mi}$; and 3) nonconservative loads are possible in the external force ${}'F_{Ni}$ if the magnitude or direction of ${}'p_i$ is dependent on displacements, for example, pressure.

In pressurized membranes, nonconservative loads occur during large displacements. The tractions ${}'p_i$ due to net pressure p normal to the membrane surface ${}'C$ are

$${}'p_i = \sqrt{{}'A/A}\,p({}'\hat{N}\cdot\hat{\boldsymbol{e}}_i) \tag{10}$$

where the dot between ${}'\hat{N}$ and $\hat{\boldsymbol{e}}_i$ represents the inner vector product of the unit normal to the surface with the Cartesian base vector $\hat{\boldsymbol{e}}_i$. Because ${}'\hat{N}$ is defined in terms of the cross product of the deformed base vectors, we replace ${}'y_i = y_i + {}'u_i$ by Eqs. (1) and find that for pressure loading Eq. (9d) becomes

$${}'F_{Ni} = pe_{kji}\left(\int\int H_N H_{Q,1}H_{M,2}\,\mathrm{d}x_1\,\mathrm{d}x_2\right)\times(Y_{Qk}Y_{Mi} + Y_{Qk}\,{}'D_{Mj} + Y_{Qk}\,{}'D_{Mj} + {}'D_{Qk}\,{}'D_{Mj}) \tag{11}$$

where e_{kji} is the permutation symbol introduced because of the cross product. We see that ${}'p_i$ and, hence, ${}'F_{Ni}$ are indeed nonlinear in the displacement components ${}'D_{Mi}$.

To evaluate the matrices in Eqs. (9), we must integrate products of the shape functions $H_M(x_\alpha)$ and their derivatives over the area of each element. Because of the complexities of those products, the integrations must be done numerically.[21] Gaussian quadrature can be used for the quadrilateral elements, and Gauss–Hammer formulas can be used for the triangular elements.

C. Nonlinear Forced Vibrations

Here we will develop a solution scheme for predicting the nonlinear dynamic motions. The scheme is a combined incremental and iterative method. We adopt a total Lagrangian approach[19] in which we disregard nonlinear interactions of the membrane with the embedding medium. If we consider the surface ${}^{\#}C$ at a slightly later time $t + \Delta t$ from the surface ${}'C$ at time t when we assume all variables are known, we can rewrite Eq. (9) at time $t + \Delta t$ as

$$[M]\{{}^{\#}\ddot{D}\} + \{{}^{\#}R\} = \{{}^{\#}F\} \tag{12}$$

where a bracketed term, for example, $[M]$, denotes a matrix, for example, M_{MNij}, and braces about a term, for example, $\{{}^{\#}R\}$, denote a vector, for example, ${}^{\#}\boldsymbol{R}_{Ni}$. The vectors $\{{}^{\#}R\}$ and $\{{}^{\#}F\}$ are obtainable from Eqs. (9) by replacing the superscript $'$ by ${}^{\#}$. Note that $[M]$ is neither dependent on time nor on displacements and, therefore, needs to be calculated only once.

If we assume that the exact value of $\{{}^{\#}D\}$ at time $t + \Delta t$ is given by an iteration on a prior estimate $\{{}^{\#}\tilde{D}\}$ to the solution, that is,

$$\{{}^{\#}D\} = \{{}^{\#}\tilde{D}\} + \{{}^{\#}\Delta D\} \tag{13a}$$

then we can take Taylor expansions in Eqs. (12) about the solution $\{{}^{\#}\tilde{D}\}$ and obtain a Newton–Raphson iterative equation[22]:

$$[M]\{{}^{\#}\ddot{D}\} + \{{}^{\#}K\}\{{}^{\#}\Delta D\} = (\{{}^{\#}\tilde{F}\} - \{{}^{\#}\tilde{R}\}] \tag{13b}$$

in which $\{{}^{\#}\tilde{F}\} - \{{}^{\#}\tilde{R}\}$ is evaluated at $\{{}^{\#}\tilde{D}\}$ and $\{{}^{\#}\tilde{K}\}$ is the tangent stiffness matrix evaluated at $\{{}^{\#}\tilde{D}\}$:

$$[{}^{\#}\tilde{K}] = \frac{\partial(\{{}^{\#}\tilde{R}\} - \{{}^{\#}\tilde{F}\})}{\partial\{{}^{\#}\tilde{D}\}} \tag{13c}$$

If conservative loads are considered, $\partial\{{}^{\#}\tilde{F}\}/\partial\{{}^{\#}\tilde{D}\} = 0$. If nonconservative loads, such as pressure, are considered, $\{{}^{\#}\tilde{F}\}$ is obtained from Eq. (11) and, therefore,

$$\frac{\partial\{{}^{\#}\tilde{F}\}}{\partial\{{}^{\#}\tilde{D}\}} = pe_{kji}\left[(Y_{Qk} + {}^{\#}D_{Qk})\int\int H_N H_{Q,1}H_{M,2}\,\mathrm{d}x_1\,\mathrm{d}x_2 + (Y_{Qk} - {}^{\#}D_{Qk})\int\int H_N H_{M,1}H_{Q,2}\,\mathrm{d}x_1\,\mathrm{d}x_2\right] \tag{14a}$$

Because of the permutation symbol e_{kji}, we see that Eq. (14a) will contribute nonsymmetric terms to the tangent stiffness matrix. It is often convenient to achieve a symmetric stiffness matrix and, therefore, in one solver described in Sec. IV, the nonsymmetric terms in Eq. (14a) were disregarded, and instead the load $\{{}^{\#}F\}$ in Eq. (12) was treated iteratively to partially account for that nonlinear effect. The full nonsymmetric terms are included in another solver described in Sec. IV.

Thus, the principal term in the tangent stiffness matrix is

$$[{}^{\#}\tilde{K}] = \frac{\partial\{{}^{\#}R\}}{\partial\{{}^{\#}\tilde{D}\}} \tag{14b}$$

and is obtained by taking the indicated derivatives of Eq. (14b),

$$\tilde{K}_{MNij} = \int\int \left\{\frac{1}{2}\delta_{ij}\,{}^{\#}n^{\alpha\beta}(H_{M,\alpha}H_{N,\beta} + H_{N,\alpha}H_{M,\beta}) + \frac{1}{4}C^{\alpha\beta\eta\xi}(H_{R,\alpha}H_{N,\beta} + H_{N,\alpha}H_{R,\beta})(Y_{Ri} + {}^{\#}\tilde{D}_{Ri})(H_{Q,\eta}H_{M,\xi} + H_{M,\eta}H_{Q,\xi})(Y_{Qj} + {}^{\#}\tilde{D}_{Qj})\right\}\sqrt{A}\,\mathrm{d}x_1\,\mathrm{d}x_2 \tag{15}$$

D. Newmark's Method[19]

Given the solution on ${}'C$ at time t and the linearized iterative form of the equations of motion, Eqs. (13–15), we seek an incremental solution for the iteration $\{{}^{\#}\Delta D\}$ to the solution on ${}^{\#}C$, Toward that

end, we assume distributions for the velocities $\{^{\#}\dot{D}\}$ and accelerations $\{^{\#}\ddot{D}\}$ during the time interval from t to $t + \Delta t$ such that

$$\{^{\#}\dot{D}\} = \{^{\prime}\dot{D}\} + [(1-\alpha)\{^{\prime}\ddot{D}\} + \alpha\{^{\#}\ddot{D}\}]\Delta t \tag{16a}$$

$$\{^{\#}D\} = \{^{\prime}D\} + \{^{\prime}\dot{D}\}\Delta t + \left[\left(\tfrac{1}{2}-\beta\right)\{^{\prime}\ddot{D}\} + \beta\{^{\#}\ddot{D}\}\right]\Delta t^2 \tag{16b}$$

where α and β are parameters dictating the assumed distribution of acceleration over the interval; different explicit and implicit formulations can be developed with different parameters. If α is equal to or greater than 0.5 and if β is equal to or greater than $0.25(0.5+\alpha)^2$, the formulation is implicit.[19]

In the implicit formulation, Eq. (16b) is solved for $\{^{\#}\ddot{D}\}$ in terms of values at time t and in terms of $\{^{\#}D\}$. On substitution into Eqs. (13), an equivalent static problem is derived at each time step in the form

$$[K_{\text{eff}}]\{^{\#}\Delta D\} = \{\tilde{F}\} - \{R_{\text{eff}}\} \tag{17a}$$

where

$$[K_{\text{eff}}] = [^{\#}K] + [M]/(\beta\Delta t^2) \tag{17b}$$

is the effective stiffness matrix and $\{\tilde{F}\} - \{R_{\text{eff}}\}$ is the similarly modified load vector.

E. Damping

Artificial damping of results, particularly of higher modes of vibration, can be realized by varying the Newmark parameter α in Eqs. (16). If $\alpha = 0.5$, no artificial damping is introduced. For increasingly larger values of α beyond 0.5, increasingly rapid artificial damping is achieved. This would be desired if steady-state, rather than transient, solutions are sought.

If real damping is present in the system, or an alternative artificial damping mechanism is sought, Rayleigh damping proportional to the stiffness and mass matrices can be introduced. Add a damping term $[^{\#}C]\{^{\#}\dot{D}\}$ to Eq. (15) with the damping matrix assumed to have the form[23]

$$[^{\#}C] = \eta[M] + \lambda[^{\#}K] \tag{18a}$$

and then add appropriate terms to $[K_{\text{eff}}]$ and $\{R_{\text{eff}}\}$. For larger values of η, the lower transient modes are more heavily damped. For larger values of λ, the higher transient modes are more heavily damped. The damping ratio ξ relative to critical damping of a particular modal frequency ω is given in terms of η and λ by[19]

$$\xi = \eta/(2\omega) + \lambda\omega/2 \tag{18b}$$

IV. Computer Implementation

The SD theory described in the preceding section has been implemented in a general purpose FORTRAN computer code, called TENSION, for analysis of the nonlinear dynamic response of cable and membrane structures. Numerous special features have been added to this code to facilitate computer simulation of parachute dynamics. A custom pre- and postprocessor written in MATLAB® has also been developed to provide for state-of-the-art model generation and visualization of the simulation results.

TENSION currently has three dynamic solvers. Two implicit solvers are based on Newmark's method, and the third is based on the explicit central difference method,[19] which is a conditionally stable method. The difference between the two implicit solvers is in the method used to solve the algebraic equations given by Eq. (17a). The first uses a direct factorization method[21] with a profile reduction algorithm[24] and is only applicable to symmetric systems, and the second employs an iterative method[25,26] that can be used for nonsymmetric systems of equations.

V. Results

In this section, three example problems are presented to demonstrate the capabilities of TENSION for simulating parachute dynamics. All three problems are performed as standalone SD simulations. The fluid effects are approximated by prescribing representative pressures on the canopy membranes and by including velocity dependent fluid drag forces on cables and concentrated masses.[8] All examples utilize a linear elastic material model with constant material properties. The properties used in these simulations are $E = 4.32 \times 10^6$ lb/ft^2 $= 0.207$ GPa, $\nu = 0.3$, membrane thickness $= 0.03$ mm (0.0001 ft), cable cross-sectional area $=$ 9.29 mm^2 (0.0001 ft^2), fabric density $= 309.3$ kg/m^3 (0.6 slugs/ft^3), air density $= 1.222$ kg/m^3 (0.00237 slugs/ft^3), and gravitational acceleration $= 9.81$ m/s^2 (32.2 ft/s^2).

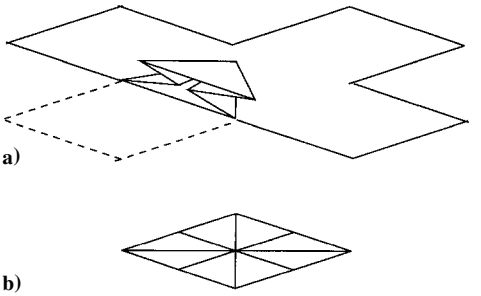

Fig. 1 Initial folded configuration of cross canopy: a) folding of one arm (upside down) and b) entire canopy.

A. Opening and Control of a Cross-Type Canopy

This example demonstrates the ability of TENSION to simulate the opening of a full three-dimensional unconstrained model of a cross-type parachute in an initially folded configuration and subsequent control of the parachute motion through user-defined changes of the control line lengths. The four arms of the cross canopy are initially folded over the canopy center, as shown for one arm in Fig. 1. In this simulation, the model is subjected to constant canopy pressure, cable and payload drag that is dependent on the square of the relative velocity, and gravity. Time-dependent mass proportional damping is applied during the initial opening to stabilize the simulation, then reduced after partial opening is achieved. The initial geometry and deformed geometries at three times during opening are shown in Fig. 2.

Following the opening, the model approaches a steady-state descent. Next, four separate control line length changes are prescribed to simulate the parachute flying in a box pattern. Control line changes are effected in the FEM model by prescribing time-dependent unstressed cable lengths. Each control operation consists of lengthening a control line for 10 s, then retracting it for 10 s prior to initiating the next control operation. The x, y, and z velocities of the payload for the entire simulation are shown in Fig. 3. Prior to control, the horizontal (x, y) velocities are zero, and terminal velocity is approached in the vertical z direction. Control operations begin at 20 s and induce the horizontal velocities shown. The trajectory of the payload is shown in Fig. 4. Here, the initial descent prior to control and the four periods of control are clearly evident. The deformed shape of the parachute model initiating the first control operation is shown in Fig. 5.

B. Opening of a Ram-Air Parafoil System

This model simulates a ram-air parafoil (wing) that is similar to that flown under the U.S. Army Guided Parafoil Airborne Delivery System (GPADS)[27] and NASA X-38[28] programs. For simplicity and reduction of computational time, the parafoil is modeled in half-plane symmetry. The wing is initially in a flat configuration that represents the cut pattern geometry. Figure 6 shows the full three-dimensional initial geometry.

The pressure distribution used in this simulation is constant for all time. This is possible due to time-dependent mass proportional damping that is slowly minimized during the early portion of the simulation. The top, bottom, and side faces are supplied different pressure distributions. The system is acted on by a gravitational load in the negative z direction, mass proportional damping, and velocity-dependent cable drag.

The time-dependent mass proportional damping is ramped from an initially high value to a low value over the first 5 s of the simulation. These values allow for a slow oozing of the parafoil into the inflated shape and a method of allowing the suspension lines, all of which start in a slack state, to become axially loaded. The program

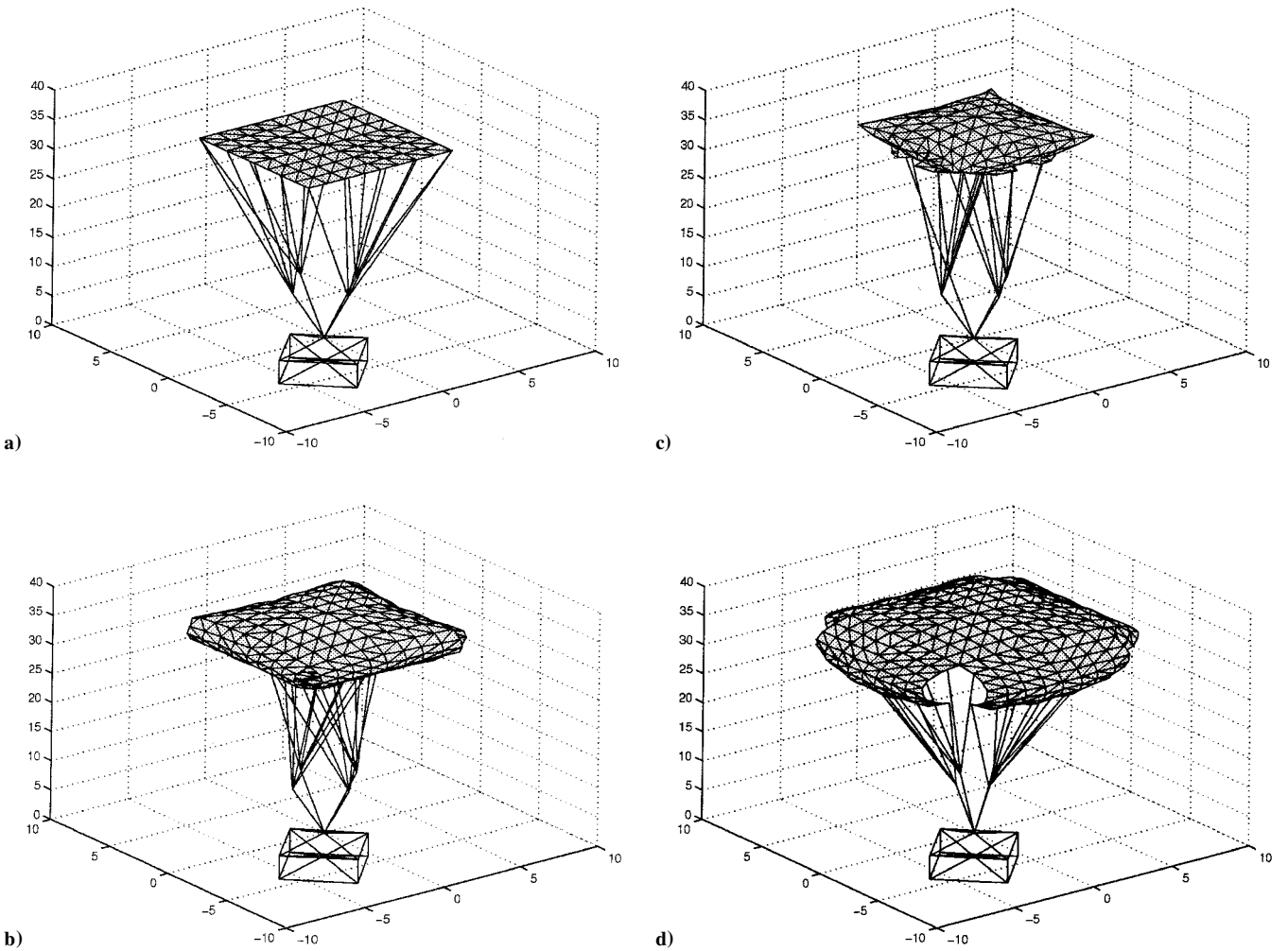

Fig. 2 Opening of cross parachute: a) initial configuration, b) first opening configuration, c) second opening configuration, and d) third opening configuration.

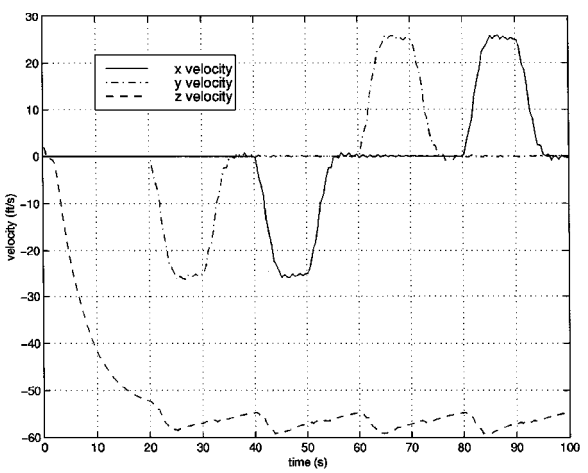

Fig. 3 Payload velocity of cross parachute.

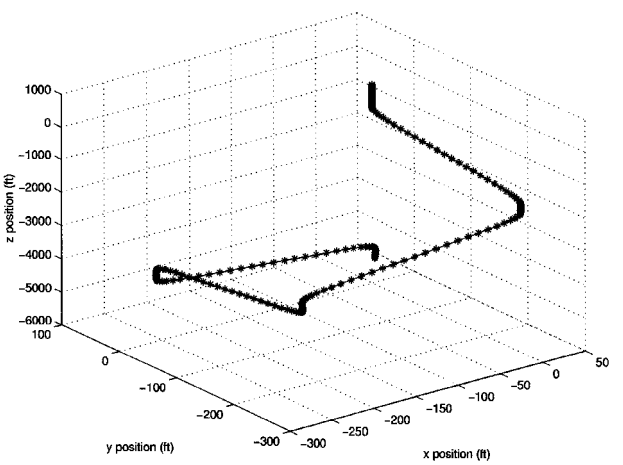

Fig. 4 Trajectory of payload of cross parachute.

allows the user to define the cable length between two nodes to be longer than the actual distance between the nodes and to prescribe that the cable is in a slack state. This is a critical capability that allows the user to run the same model (same nodal coordinates) with different sets of suspension line and bridle lengths. The user can also prescribe changes in cable lengths in time that could be used to predict the effect on the systems performance to changes in rigging angle. As already mentioned, all suspension lines are initially in a slack state with a user-defined cut length. This also assists in model development due to the relatively simple geometry and the ability to incorporate actual cut patterns for the canopy. The time-dependent mass proportional damping allows for the smooth transition to an inflated shape and transition into steady-state glide. Figure 7 shows a sequence of snapshots during the initial inflation process.

The system slowly reaches a steady-state glide after approximately 40 s. Figure 8 shows the y and z positions of the payload and node A vs time. At a simulation time of 45 s, six trailing-edge control lines are shortened to a predefined length over a 5-s time interval to simulate a flare maneuver. The pressure loading on the

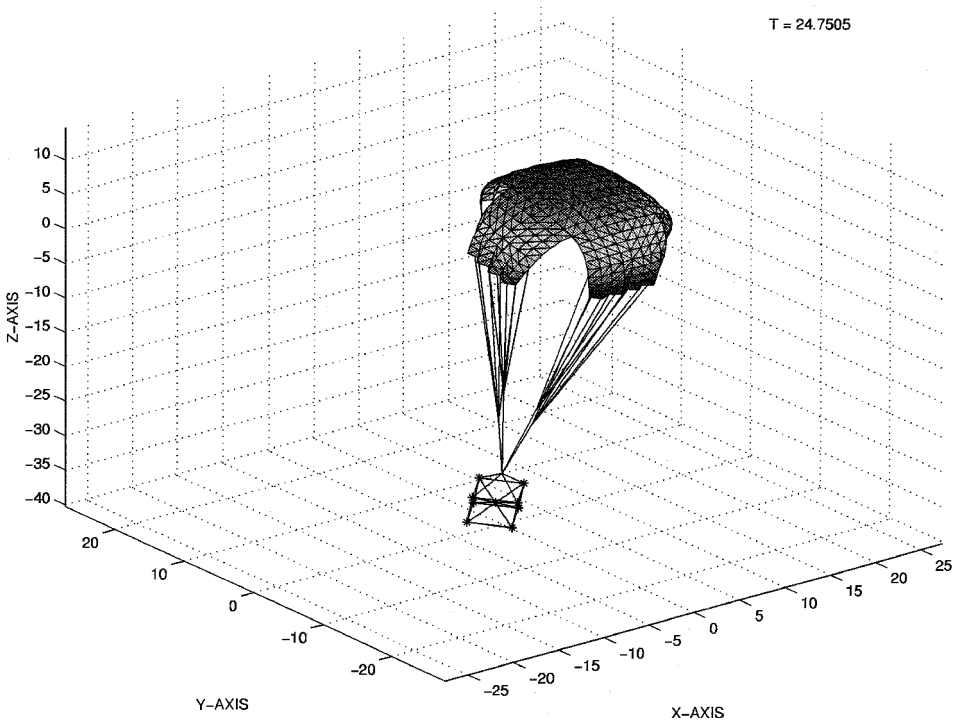

Fig. 5 Deformed shape of cross parachute during first control operation.

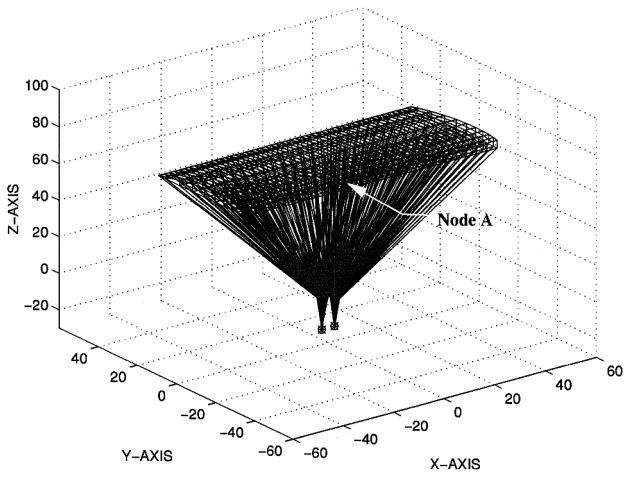

Fig. 6 Initial geometry of parafoil model.

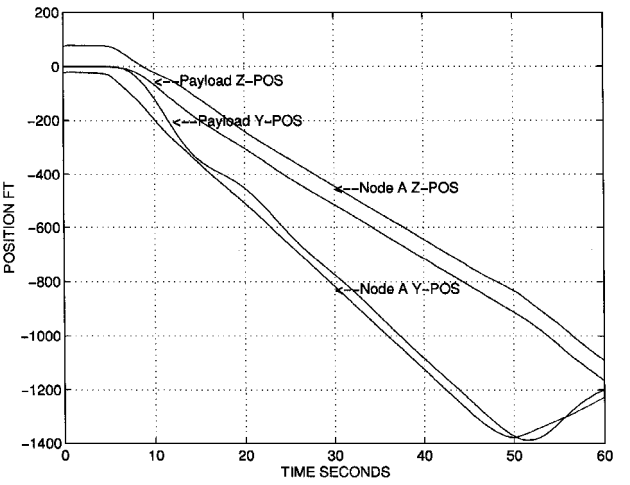

Fig. 8 Position vs time curves for parafoil simulation.

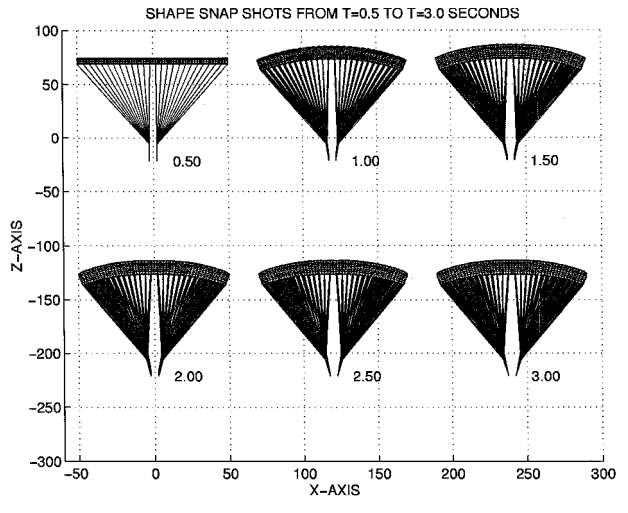

Fig. 7 Deformed shapes during parafoil inflation.

system during a flare will most definitely change over time; however, for this simulation, the pressure is assumed constant. The y and z velocities of the payload and node A are shown in Fig. 9, which clearly shows the effect of the flare maneuver.

This example demonstrates the ability of TENSION to simulate the inflation of a parafoil starting from cut patterns to a steady-state glide with the potential of the user modifying the rigging angle in time to optimize design and a flare-type control maneuver. Generalization to a fully three-dimensional unconstrained model for turn performance predictions is expected to be a small modification that would simply increase the overall model size.

C. Opening of a Round Canopy

The third example is a generic round ring-slot canopy. The model consists of 28 gores and 6 ring slots. The model starts in a folded configuration, as shown in Fig. 10. The simulation begins with an initial horizontal velocity on all node points in the negative x direction. Note that all 28 gores are folded along the gore centerlines in a configuration that is close to that obtained at line stretch. The model is fully three-dimensional and unconstrained.

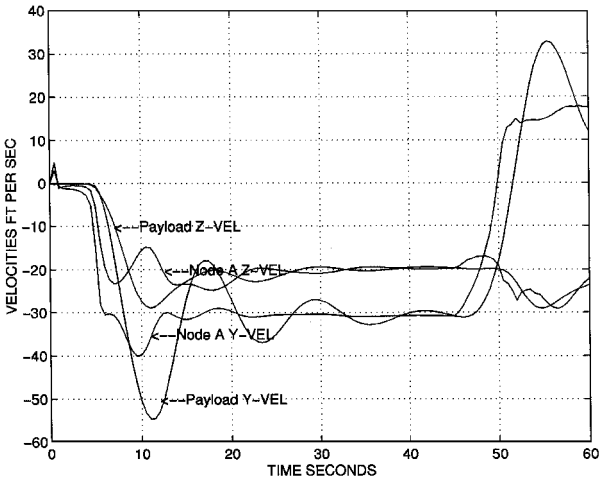

Fig. 9 Velocity vs time curves for parafoil simulation.

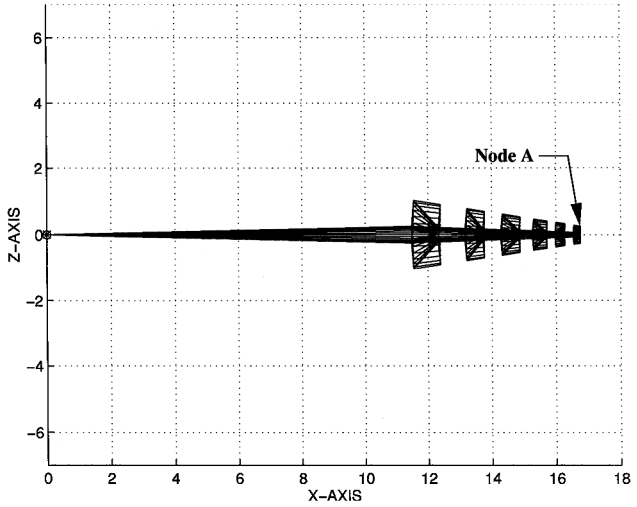

Fig. 10 Initial folded configuration of ring-slot parachute.

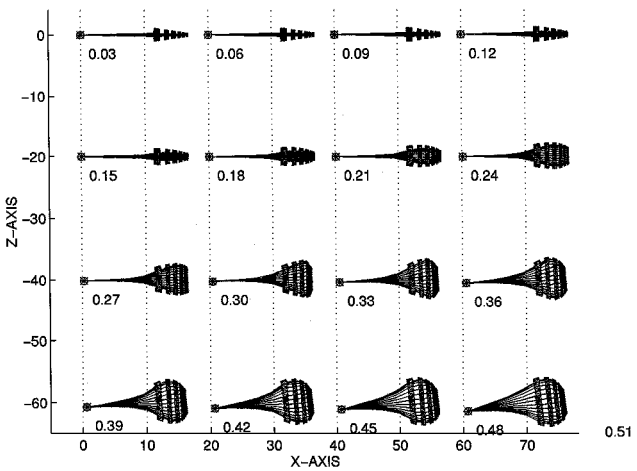

Fig. 11 Deformed shapes of ring-slot parachute during inflation (0.03–0.48 s).

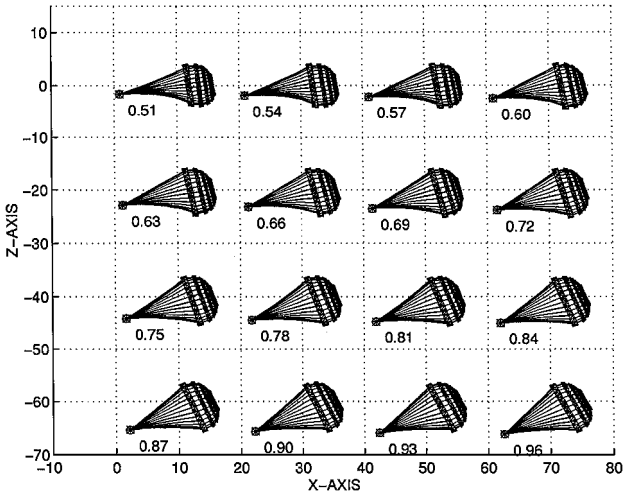

Fig. 12 Deformed shapes of ring-slot parachute during inflation (0.51–0.96 s).

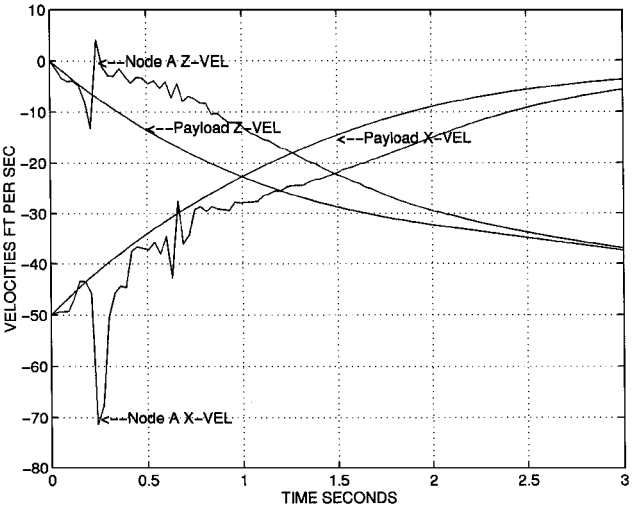

Fig. 13 Velocity vs time curves for ring-slot parachute.

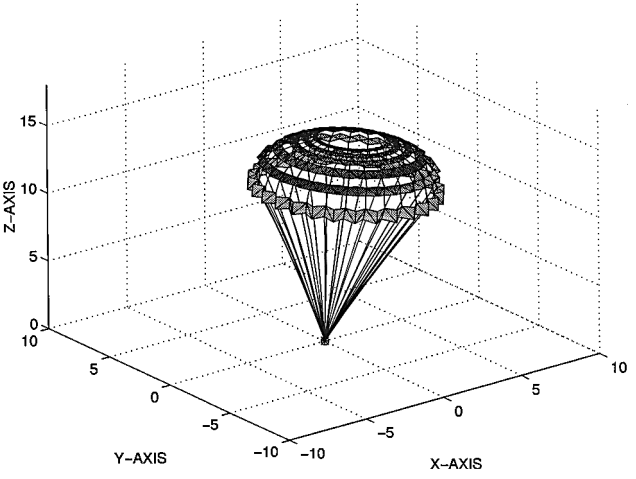

Fig. 14 Final shape of ring-slot parachute.

The model is subjected to a vertical gravitational loading, user-defined time-dependent pressure distribution, velocity-dependent cable drag, and velocity-dependent payload drag. Time-dependent mass proportional damping is minimally present over the first 4 s of the simulation.

A time-dependent outward acting pressure distribution is simultaneously applied to all membrane elements. Gravity is acting throughout the simulation. The seam cables, suspension line cables, and payload are subjected to velocity-dependent drag loads for all times, which assists in the trajectory changing from pure horizontal motion to pure vertical motion.

A sequence of payload-fixed snapshots are shown in Figs. 11 and 12 for time intervals of 0.03–0.48 and 0.51–0.96 s, respectively. These snapshots clearly show the three-dimensional capabilities of TENSION. For example, the uppermost suspension lines become stressed and elongated during the inflation before the lowermost suspension lines. The lower suspension lines also appear to be most visibly affected by the fluid drag. Figure 13 shows the

horizontal and vertical velocities of the payload and node A vs time. The system's final shape is shown in Fig. 14.

This model demonstrates the ability of TENSION to simulate a round canopy with an initial horizontal velocity and folded configuration through opening and ultimately into a steady-state vertical terminal configuration.

VI. Conclusions

The finite element formulation for an SD model capable of simulating the nonlinear dynamic behavior of highly flexible structures comprising membranes and cables has been presented. This model is currently being used to simulate the inflation, terminal descent, and control of a variety of parachute systems. Three example problems were presented to demonstrate the capabilities of this model for simulating parachute dynamics. In these examples, the effect of the surrounding airflow was approximated by prescribing the membrane pressure and cable and payload drag on the structural model. Coupling of the structural model with CFD programs has been presented in other publications.[14,15] The ultimate goal of these efforts is to be able to design and optimize parachute systems using computer simulations, reduce the life cycle costs of airdrop systems, and provide an airdrop virtual proving ground.

Acknowledgments

This material is based on work supported in part by the U.S. Army Research Office under Grant DAA04-96-1-0051 and in part by the U.S. Air Force Office of Scientific Research under Grant F49620-98-1-0214 to the University of Connecticut.

References

[1]Strickland, J. H., and Higuchi, H., "Parachute Aerodynamics: An Assessment of Prediction Capability (1995)," AIAA Paper 95-1531, May 1995.

[2]Knacke, T. W., "Parachute Recovery Systems Design Manual," Naval Weapons Center, NWC TP 6575, China Lake, CA, June 1987.

[3]Purvis, J. W., "Improved Prediction of Parachute Line Sail During Lines-First Deployment," AIAA Paper 84-0786, April 1984.

[4]Sundberg, W. D., "Finite-Element Modeling of Parachute Deployment and Inflation," AIAA Paper 75-1380, Nov. 1975.

[5]Haug, E., Lasry, D., and de Kermel, P., "Dynamic Simulation of Industrial Membranes Including Their Interaction with Surrounding Media," *Third International Symposium of the SFB 230 "Evolution of Natural Structures,"* Univ. of Stuttgart, Stuttgart, Germany, Oct. 1994.

[6]Stein, K., Benney, R., Kalro, V., Johnson, A., and Tezduyar, T., "Parallel Computation of Parachute Fluid–Structure Interactions," AIAA Paper 97-1505, June 1997.

[7]Mosseev, Y., "The Multipurpose Integrated PC Software for Structural and Aeroelastic Analysis of Decelerators, Paragliders, and Balloons," AIAA Paper 97-1455, June 1997.

[8]Benney, R., Stein, K., Leonard, J., and Accorsi, M., "Current Three-Dimensional Structural Dynamic Finite Element Modeling Capabilities," AIAA Paper 97-1506, June 1997.

[9]Chuzet, L., "Numerical Determination of Parachutes Performances with SINPA Software," AIAA Paper 97-1509, June 1997.

[10]Sahu, J., and Benney, R., "Prediction of Terminal Descent Characteristics of Parachute Clusters Using CFD," AIAA Paper 97-1453, June 1997.

[11]Kalro, V., Gerrard, W., and Tezduyar, T., "Parallel Finite Element Simulation of the Flare Maneuver of Large Ram-Air Parachutes," AIAA Paper 97-1506, June 1997.

[12]Lacroix, C., Ibos, C., Chuzet, L., and Granville, D., "SINPA-A Full Three-Dimensional Fluid–Structure Software for Parachute Simulation," AIAA Paper 97-1508, June 1997.

[13]Nelsen, J. M., "Computational Fluid Dynamics Studies of a Solid and Ribbon 12-Gore Parachute Canopy in Subsonic and Supersonic Flow," AIAA Paper 95-1558, May 1995.

[14]Stein, K., Benney, R., Kalro, V., Tezduyar, T., Leonard, J., and Accorsi, M., "Parachute Fluid–Structure Interactions: 3-D Computation," *Computer Methods in Applied Mechanics and Engineering* (to be published).

[15]Benney, R., Stein, K., Kalro, V., Tezduyar, T., Leonard, J., and Accorsi, M., "Parachute Performance Simulations: A 3D Fluid–Structure Interaction Model," 21st Army Science Conf., Paper C-04, Norfolk, VA, June 1998.

[16]Stein, K., Benney, R., Kalro, V., Tezduyar, T., Bretl, T., and Potvin, J., "Fluid–Structure Interaction Simulations of a Cross Parachute: Comparison of Numerical Predictions with Wind Tunnel Data," AIAA Paper 99-1725, June 1999.

[17]Leonard, J. W., *Tension Structures*, McGraw–Hill, London, 1988, Chap. 8.

[18]Lo, A., "Nonlinear Dynamic Analysis of Cable and Membrane Structures," Ph.D. Dissertation, Civil Engineering Dept., Oregon State Univ., Corvallis, OR, June 1982.

[19]Bathe, K. J., *Finite Element Procedures*, Prentice–Hall, Upper Saddle River, NJ, 1996, Chaps. 5 and 6.

[20]Green, A. E., and Adkins, J. E., *Large Elastic Deformations and Nonlinear Continuum Mechanics*, Oxford Univ. Press, Oxford, 1960, 2nd ed., 1970, Chaps. 1 and 2.

[21]Atkinson, K. E., *An Introduction to Numerical Analysis*, 2nd ed., Wiley, New York, 1989, Chaps. 5, 7, and 8.

[22]Oden, J. T., *Finite Elements of Nonlinear Continua*, McGraw–Hill, New York, 1972, Chap. 5.

[23]Clough, R. W., and Penzien, J., *Dynamics of Structures*, McGraw–Hill, New York, 1975, Chap. 13.

[24]Sloan, S. W., "A FORTRAN Program for Profile and Wavefront Reduction," *International Journal for Numerical Methods in Engineering*, Vol. 28, No. 11, 1989, pp. 2651–2679.

[25]Saad, Y., and Schultz, M., "GMRES: A Generalized Minimal Residual Algorithm for Solving Nonsymmetric Linear Systems," *SIAM Journal on Scientific and Statistical Computing*, Vol. 7, No. 3, 1986, pp. 856–869.

[26]Kennedy, J. G., Behr, M., Kalro, V., and Tezduyar, T., "Implementation of Implicit Finite Element Methods for Incompressible Flows on the CM-5," *Computer Methods in Applied Mechanics and Engineering*, Vol. 119, No. 1–2, 1994, pp. 95–111.

[27]Wailes, W., and Harrington, N., "The Guided Parafoil Airborne Delivery System Program," AIAA Paper 95-1538, May 1995.

[28]Machin, R., Stein, J., and Muratore, J., "An Overview of the X-38 Prototype Crew Return Vehicle Development and Test Program," AIAA Paper 99-1703, June 1999.

S. Saigal
Associate Editor